A first-principles study of C_3N nanostructures : control and engineering of the electronic and magnetic properties of nanosheets, tubes and ribbons

A EUROPEAN JOURNAL

CHEMPHYSCHEM

OF CHEMICAL PHYSICS AND PHYSICAL CHEMISTRY

Accepted Article

Title: A first-principles study of C3N nanostructures: Control and engineering of the electronic and magnetic properties of nanosheets, tubes and ribbons

Authors: Asadollah Bafekry, Catherine Stampfl, and saber Shayesteh

To be cited as: *ChemPhysChem* 10.1002/cphc.201900852

Link to VoR: http://dx.doi.org/10.1002/cphc.201900852

A Journal of

ChemPubSoc Europe

WILEY-VCH

www.chemphyschem.org

A first-principles study of C_3N nanostructures: Control and engineering of the electronic and magnetic properties of nanosheets, tubes and ribbons

A. Bafekry,[1,2] C. Stampfl,[3,*] and S. Farjami Shayesteh[1]

[1]*Department of Physics, University of Guilan, 41335-1914 Rasht, Iran*

[2]*Department of Physics, University of Antwerp, Groenenborgerlaan 171, B-2020 Antwerp, Belgium*

[3]*School of Physics, The University of Sydney, New South Wales 2006, Australia*

Abstract

Using first-principles calculations we systematically investigate the atomic, electronic and magnetic properties of novel two-dimensional materials (2DM) with a stoichiometry C_3N which has recently been synthesized. We investigate how the number of layers affect the electronic properties by considering monolayer, bilayer and trilayer structures, with different stacking of the layers. We find that a transition from semiconducting to metallic character occurs which could offer potential applications in future nanoelectronic devices. We also study the affect of width of C_3N nanoribbons, as well as the radius and length of C_3N nanotubes, on the atomic, electronic and magnetic properties. Our results show that these properties can be modified depending on these dimensions, and depend markedly on the nature of the edge states. Functionalization of the nanostructures by the adsorption of H adatoms is found induce metallic, half-metallic, semiconducting and ferromagnetic behavior, which offers an approach to tailor the properties, as can the application of strain. Our calculations give insight into this new family of C_3N nanostructures, which reveal unusual electronic and magnetic properties, and may have great potential in applications such as sensors, electronics and optoelectronic at the nanoscale.

I. INTRODUCTION

Two-dimensional materials (2DM) have attracted significant scientific attention because of their variable chemical compositions and promising electronic properties for a wide range of technological applications. Recently, a large subgroup of 2D crystals has attracted intense attention, namely a special class of 2D carbon nitride (2DCN) nanomaterials due to their anisotropic 2D geometric morphology, which can be stabilized as monolayers by taking advantage of the multifarious chemistry of C and N, as well as their promising electronic properties for wide range applications.[1–6] The 2DCN nanosheets including C_2N,[7,8] C_3N_4,[9–11] C_4N_3,[12–14] C_6N_6,[15–18] C_6N_7,[19–22] have already been synthesized in experiments and were found to have unique properties, and hold promise for numerous application by tuning the band gap.[3,7,23,24] In addition to those structures mentioned above, C_3N_2[25,26] C_2N_2, C_4N[27] C_8N_2,[28] C_9N_4,[29] C_9N_7,[30] $C_{10}N_9$ and $C_{14}N_{12}$,[31] C_3N_5,[32] nanosheets have also been theoretically proposed, which possess interesting electronic and topological properties as functional carbon nitrides. Versatile electronic and magnetic properties are found in these carbon nitrides, which are related to the holey geometrical character.[33–36] Very recently, 2D polyaniline with stoichiometric formula C_3N has been successfully synthesized.[37] The monolayer C_3N was first reported to be a semiconductor and three possible planar structures were suggested.[38,39] Successful experimental synthesis of C_2N and C_3N consequently raised the importance of the evaluation of their intrinsic properties.[40–42]

The C_3N material, as a novel 2DM with semiconducting electronic properties, is well suited for numerous applications in, e.g., solar cell devices, electrolyte gating and doping of transistors and anode materials.[43–45] The electronic structure of the C_3N nanosheet can be tailored by vacancy defects and surface decoration, which convert it into a metal or a magnetic semiconductor.[42,46–53] As a member of the graphene-like materials, however, no evidence for the electronic properties and formation of magnetic order in C_3N nanoribbons have been reported so far. Because the 2D nanosheet can be regarded as a precursor of one-dimensional (1D) nanomaterials, which would be cut into nanoribbons or rolled into nanotubes,[54–56] the discovery of C_3N nanosheets also generates interest in its 1D-forms, that is, C_3N nanoribbons and nanotubes. Obtaining a comprehensive understanding of the physical and chemical properties of C_3N nanostructures plays a crucial role in their future potential applications in nanodevices. Despite the fact that two-dimensional materials (2DM) hold great potential for a wide range of applications, it will be necessary to

modulate their intrinsic properties. Several approaches have been developed to modify the electronic properties of 2DM, which these methods involve substitutional doping, defect engineering, surface functionalization with adatoms, application of an electric field or strain, and by affecting the edge states. Many efforts have been put forth on band gap modification methods of 2DM including the adsorption and substitution of atoms, different defects and strain.[57–66,68]

In this paper, we first investigate the layer thickness-dependence of the electronic properties of the C_3N nanosheet (NS)(C_3NNS). Single layers of C_3NNS can be stacked together to form a few layer C_3NNS structure with multiple types of stacking configurations. Our results show, depending on layer thickness and type of stacking, that the band structure can exhibit a metallic or semiconducting behavior. The C_3N nanoribbon (C_3NNR) and nanotube (C_3NNT) are characterized by a change in electronic character depending on the width, length and radius and with respect to the zigzag and armchair edges. The character of these nanostructures in either shape can be tuned through changing the width of the nanoribbon or length/radius of the nanotube. Moreover, we investigate the adsorption of H adatoms on the C_3N nanostructures, as well as the effects of charging and strain on the electronic structure, where we find that the band gap and magnetism can be modulated and tuned.

II. METHOD

In this work, we performed first-principles calculations, using the generalized gradient approximation (PBE-GGA)[69] for the exchange-correlationfunctional and norm-conserving pseudopotentials.[70] The wave functions are expanded in a linear combination of pseudo atomic orbitals (LCPAOs) generated by using a confinement scheme.[71,72] The **k**-point mesh for sampling over the Brillouin zone (BZ) integration is generated using the Monkhorst-Pack scheme.[73] For a primitive unit cell of hexagonal C_3N, a **k**-mesh grid of $15 \times 15 \times 1$ was used. After the convergence tests, we chose cutoff of 300 Ry for C_3N nanosheet, so that the total energy converged to below 1.0 meV/atom. The geometries were fully relaxed until the force convergence acting on each atom was less than meV/Å. Simulated scanning tunneling microscopy (STM) images were obtained using the Tersoff-Hamann theory[74] for STM images, as implemented in the OpenMX code, and were plotted using WSxM software.[75]

III. THE C_3N NANOSHEET

The geometric structure of planar, monolayer C_3N with lattice constant 4.861 Å is shown in Fig. 1(a). The bond lengths of C-C and C-N are 1.404 and 1.403 Å, respectively. These results are in good agreement with previous reports.[37,39?] The difference charge density is calculated by subtracting the charge densities of free C and N atoms from the charge density of C_3N and is shown together with the total charge density in Fig. 1(a). The difference charge density shows electron density accumulation around the N atom, indicating charge transfer from C to N atoms. The Bader charge analysis is performed using the Quantum Espresso code.[76] Our results show that each N atom gains about 0.6 electrons from the adjacent C atoms. The charge redistributions are due to the different electro-negativities of the C and N atoms. In order to provide visible guidance for experimental observations, we present calculated STM images (Fig. 1(a)). To produce the calculated STM image, the Kohn Sham charge density is integrated at a voltage of +2.0 V. It can be seen that the brightest spots occur in the regions around the C bonds. From the predicted STM images, it is easy to recognize and correlate them with the corresponding atomistic structure.

The density of states (DOS) and partially DOS (PDOS) of C_3N are shown in Fig. 1(b). Since in C_3N two C atoms are replaced by N relative to graphene, the p_z orbital band is fully occupied by the additional two electrons, leading to a semiconducting behavior with a band gap between the C-p_z states forming the Dirac-point which is lowered by 2.25 eV relative to the Fermi energy, E_F. From the PDOS, we can see that the valence band maximum (VBM) of C_3N is predominately composed of N-p_z orbitals and the Dirac-point is thus formed by N-p_z states, whereas the conduction band minimum (CBM) is dominated by C-p_z orbital states. Our calculations are in agreement with previous studies.[37,38,77] The orbital-projected band structure of C_3N, is shown in Fig. S1 (supplementary information (SI)). Our calculations show that C_3N is an indirect band gap semiconductor (0.4 eV), where the VBM is located at the **M** point and the CBM is at the Γ point.

A. Effect of Layer thickness

In the following we consider bilayers of C_3N (2L-C_3N) with two different stacking sequences of AA and AB. In the AA stacking, the in-plane position of atoms in the two layers are exactly the same, while in the AB stacking, the in-plane atomic positions of the top layer

are shifted such that some of the atoms are placed on the hollow center of the hexagonal lattice of the atoms of the bottom layer. In the tri layer C_3N (3L-C_3N), sandwich structure, we consider four stacking configurations: AAA, ABA, ABB and AAB. In the ABA stacking configuration, a hexagonal ring center and a C atom are located directly below and above the C atom of the C_3N lattice, respectively; and a N atom and a hexagonal ring center are located directly below and above the C atom of the C_3N lattice, respectively. The optimized atomic structure of 2L- and 3L-C_3NNS, are shown in Fig. 2(a-f), respectively. After geometry optimization, the interlayer distances between the layers of 2L-C_3N, are obtained as 3.309 (AA)and 3.298 Å (AB), while for 3L-C_3N, the distances are 3.301 (AAA), 3.305 (ABA), 3.587 (ABB) and 3.316 (AAB) Å,. For the 2LAA- and 2LAB-C_3N structures, the in-plane covalent bond lengths of the C-C and C-N atoms are 1.398 and 1.408 Å, respectively, and can be compared to the C_3N respective bond lengths of C-C and C-N of1.403 and 1.404 Å). For 3L-C_3N, the in-plane covalent bond length of the C-C and C-N atoms is $\sim$ 1.40 Å.

The electronic structure of 2L- and 3L-C_3N, is shown in Figs. 2(a-f). We find that the energy band structure of C_3N is modified by the number of layers and type of stacking configuration. Our results show that the 2LAA structure eliminates the semiconducting band gap of C_3N and exhibits a metallic character, while the 2LAB structure, becomes an indirect semiconductor with a 0.45 eV band gap, where the VBM and CBM are located at the Γ and **M** points, respectively. The 3L-C_3N structure exhibits a metallic character for all stackings except the 3LABA, which becomes an indirect semiconductor with a band gap of 0.5 eV. Compared to the monolayer C_3N nanosheet (band gap 0.4 eV), the band gaps of bilayer (AA) and trilayer except ABA) are pronouncedly reduced because of the strong interlayer interaction.[78,79]

B. Effect of electric field

Here we investigate the effect of a uniform electric field on the electronic properties of bilayer C_3NNS under a perpendicular electric field $\mathbf{F} > 0$ and < 0 that denotes parallel and antiparallel to the z-axis, respectively The electronic structure, under an electric field of -0.8 to $+0.8\mathrm{V}/\mathring{A}$, is shown in Fig. 3(a). We find that the electric field changes the electronic structure of bilayer C_3NNS and brings out a redistribution of molecular orbitals as well as a reduction in the gap between frontier orbitals. The results (Fig. 3(b)) show that when an

electric field is applied the band gap decreases and reaches zero as the electric field increases (both parallel and antiparallel to the z-axis) and a semiconductor-to-metal transition occurs. Thus, it is possible to tune the electronic properties by controlling the Fermi-level via an electric field. The optimized atomic structure of bilayer C_3NNS is indicated in the inset. Owing to the tunable band gap over a wide range, the layered C_3NNS materials may provide tremendous opportunities to be applied in nanoscale electronic and optoelectronic devices.

IV. C_3N NANORIBBONS

With respect to the C_3NNR, although there is a previous report on C_3N nanoribbons,[80] the investigated structure does not correspond to the experimentally synthesized C_3N ordered arrangement. The C_3N nanoribbon (C_3NNR) formed from a C_3N nanosheet are structures that show rich properties and character due to its edge states and width effects providing important features for various technological applications. By cutting a C_3NNS along the x or y directions we obtain the C_3NNR with two types of edge configurations. Two major families of C_3NNR are distinguished depending on their orientations, namely, armchair and zigzag nanoribbons. Apart from the orientation, C_3NNR are specified according to their widths, characterized in terms of a number n of C-N bases in the unit cells. For armchair nanoribbons, the width, n, is defined by the number of C-N or C-C chains in the unit cell which are parallel to the axis of the nanoribbon; for zigzag nanoribbons, n denotes the number of zigzag C-N or C-C chains along the nanoribbon axis. For convenience, they are specified as nZ-C_3NNS and nA-C_3NNS, respectively. Hence, n indicates C_3NNR having n C-N pairs in their unit cell. Dimer lines across the widths are employed to determine the width (W_Z and W_A) of zigzag and armchair edged C_3NNR, respectively. In the present paper, we investigate both the zigzag and armchair edge nanoribbons. The atomic structures of the nanoribbons, which are passivated by hydrogen atoms, in the I and II configurations, are shown in Figs. 4(a-d). The total and difference charge density, are shown in the same panel. Similar to the C_3NNS, the bonding between atoms in the C_3NNR with zigzag and armchair edges is covalent in nature. The charge density of zigzag and armchair edge states confirm their localization at the edges.

A. Effect of nanoribbon edge states

The band gap of C_3N*NR* can differ from that of C_3N*NS* due to the combined effects of quantum confinement, edge state bands as well as folding in the direction perpendicular to the *NR* axis. We find that the band gap of the C_3N*NR* depends on its width given by n and type of edge states. Here, we investigate the electronic and magnetic properties of nZ- and nA-C_3N*NR* with n= 4 and 5 for the I and II configurations. The optimized and electronic structures, are presented in Figs. 5(a,b). We see that the 4Z-C_3N*NR* exhibits a metallic (in I and II) and an indirect semiconductor character with a 90 meV band gap (in II). Interestingly, the 5Z-C_3N*NR*, becomes a half-metal (in I and II) with an indirect band gap of 0.55 eV in the $\downarrow$ spin channel. In addition, the degeneracy of $\uparrow$ and $\downarrow$ spin channels is broken and triggers a magnetic moment of 1.0 μ_B. This suggests that the charge carriers within the energy bands around E_F are mobile, which is useful for conductive behavior and magnetic coupling. We note that the half-metallic behavior can be quite important for application in spintronics. For the nA-C_3N*NR* with n= 4 and 5 (in I and II), the systems remain an indirect semicounductor with a band gap in the range of 1.2-1.5 eV (see Fig. 5(b)). Our calculations show that the band structure of the ribbon appears to strongly depend on its width and is sensitive to the type of configuration and exhibits diverse electronic and magnetic properties. This offers an approach to tune the band gaps of nanomaterials, by changing the width and configuration.

B. Effect of nanoribbon width

In the following we explore the effects of the width of nanoribbons of C_3N for the two different edge states. The electronic band structure of H-passivated nZ- and nA-C_3N*NR* with n = 4-11 for configuration I are shown in Figs. 6(a,b). The top view of the optimized atomic structures is shown as well. The band gap of the nZ- and nA-C_3N*NR*, with respect to the width, exhibits a quantum confinement effect, namely, a band-gap reduction with increasing width. It is interesting to note that as the width increases, the band gaps of the armchair and zigzag structures converge to different values, neither of which are that of the C_3N*NS*; this is due to the fact that the VBM or CBM are determined by the edge states. The electronic structure of the C_3N*NR* exhibit a family of behavior with respect to the number of dimer lines n=odd, and the family with n=even. We can see from Fig. 6(a) that

the nZ-$C_3N$$NR$ with n=even, exhibit a metallic character. In this state, one edge is the C atoms and the other edge the C and N atoms, as a result the C edge and the N edge are negatively and positively charged, respectively. Because of this polarization, the potential felt by electrons is higher at the N edge and lower at the C edge, contributing a factor which decreases the band gap since the VBM and CBM are localized at the C edge and the N edge, respectively. We find for the nZ-$C_3N$$NR$ with n=odd that they exhibit a semiconducting character, where the band gap decreases from 1.25 eV (n=4) to 0.72 eV (n=10) with increase in the nanoribbon width, and in this state, both edges contain the C and N atoms (see Fig. 6(a)). However, for nA-$C_3N$$NR$ they have reflection symmetry with respect to their axis and the band structure is dependent on the width (irrespective of whether n is even or odd). Our results show that the nA-$C_3N$$NR$ have a semiconducting charasteristic, where the band gap decreases with increasing width (n=odd=even), and reaches zero for n=11. The band structure of nA- and nZ-$C_3N$$NR$ for different widths is distinct, and thus the electronic properties strongly depend on the width. Therefore contol of the nanoribbon structures offer a way to modulate energy band gap of such nanomaterials.

V. C_3N NANOTUBES

Recently porous and low-defect graphitic carbon nitride (g-C_3N_4) nanotubes have been fabricated[81] and also decorated with Pt nanoparticles[82] where it was found that they exhibited outstanding photocatalytic H_2 production under visible light. C_xN nanotubes have also been successfully synthesized[83] and the relative stability of small C_xN nanotubes has been theoretically investigated by Hales *et al.*.[84] This work revealed that C_3N nanotubes show a distorted configuration that is free of the tube chirality.[84] Other theoretical predictions of the geometry of C_3N nanotubes are available in the literature.[85,86] Azevedo *et al.*[87] have shown that C-N bonds are more favorable than C-B bonds and therefore that the $C_3N$$NT$ is more stable than BC_3 nanotubes. The electronic properties and adsorption abilities of C_3N nanotubes have been investigated,[88,89] which indicate potential applications in chemical sensors[90,91] and hydrogen storage.[92,93] To simulate C_3N nanotubes ($C_3N$$NT$), the $C_3N$$NS$ with a flat structure is directly rolled up into the corresponding nanotube. The structural information of the nanotube is described by a pair of integer indices (n,m) that defines a roll-up vector R=na+mb, where a and b are lattice vectors of the $C_3N$$NS$. The nanotubes can be classified by chiral vectors which are specified by a pair of integer indices (n,m),

according to the rolling/chiral angles. The nanotubes with (n,0) and (n,n) configurations represent the zigzag and armchair states, respectively, and all other (n,m) configurations are chiral nanotubes. Specifically, two types of nanotube are considered in this work, namely, zigzag (n,0) and armchair (n,n). In Fig. S2 the atomic geometry of the C_3NNS with possible wrapping of zigzag and armchair chiralities and structural models of C_3NNT made of a wrapped C_3NNS is shown.

A. Effect of nanotube length

In the following we study the influence of the nanotube length where two types of nanotubes are considered, namely, zigzag nanotubes (4,0), and armchair nanotubes (4,4) which are passivated with H atoms. The top and side views of the optimized atomic structures for (4,0) and (4,4)-C_3NNT with different lengths, are shown in Figs. 7(a,b), respectively. For the (4,0)-C_3NNT, the length varies from 8.87 to 17.04 Å and for the (4,4)A-C_3NNT, they vary from 5.77 to 10.54 Å. The electronic band structures for difference length of (4,0) and (4,4)-C_3NNT, are shown in Figs. 7(c,d). From Fig. 7(c), we can see that band gap reduces and then increases for the (4,0)-C_3NNT with increasing length, while for (4,4)-C_3NNT, the band gap is reduced from 2.25 to 1 eV (see Fig. 7(d)). The different electronic band structure of the (4,0) and (4,4)-C_3NNT for different lengths is notable. These results show that the electronic properties of C_3NNT depend on the length and hence one the band gap can be modulated by contolling the length of C_3NNT.

B. Effect of nanotube diameter

In this section, we investigate the effect of the diameters of C_3NNT for two different edges (zigzag and armchair). We calculate the electronic band structure of the (n,0) and (n,n)-C_3NNT with n=4, 6, 8 and 10 for different diameters. The top and side views of the optimized atomic structures for the (n,0) and (n,n)-C_3NNT, are shown in Figs. 8(a,b). For (n,0) C_3NNT, the diameter increases from 0.3997 to 6.41 Å and for (n,n) nanotubes, from 5.43 to 13.82Å. The resulting electronic band structure of (n,0)- and (n,n)-C_3NNT for the different diameters are shown in Figs. 8(c,d). For the (n,0)-C_3NNT with varying diameters of 5.43 and 6.41 Å (n= 4 and 8), the structures becomes direct semiconductors with band gaps of 0.52 and 0.42 eV, respectively, while for diameters varying between 4.93 and 7.44 Å

(n= 6 and 10), they exhibit a metallic character. With increasing diameter of (n,0)-C_3N*NT*, we can see semiconducting and metallic characters. Whereas for the (n,n)A-C_3N*NT*, with diameters 4.93 and 7.44 Å (n= 4, 8 and 10), the nanotubes becomes semiconductors with band gap values of 0.55, 0.8eV and 0.7 eV, respectively and finally for the n= 6, structure it becomes metallic. Thus, we can see that these structures exhibit both semiconducting and metallic properties depending on the diameter. The electronic structure of nanotubes with the armchair edge exhibits a significant change, while those with the zigzag edge exhibited little change, leading to the conclusion that the band gap of armchair nanotubes edge can be easily tuned.

VI. ADSORPTION OF H ATOMS

The top and side views of the optimized atomic structures for H adsorption on C_3N*NS*, C_3N*NR* and C_3N*NT* with zigzag and armchair edge configurations, are shown in Fig. S3. We find that with the adsorption of H adatoms, local distortions can occur in the atomic structures around the H adatoms in all C_3N nanostructures. For the H/C_3N*NS*, the C atom moves out of the base planar surface and the C-C/C-N bond lengths are elongated (1.5 Å) in comparison with the C-C bond length 1.42 Å in the C_3N*NS*; also the H-C-C angles are in the range of 110°, displaying the characters of sp^3 hybridization. After relaxation, the C-H bond length is 1.12 Å. We can see that the C atoms directly below the H adatom undergoes a notable shift in the opposite direction, thus finally resulting in a buckling of 0.5 Å in the plane of the C_3N*NS*. For the H/5Z- and H/7A-C_3N*NR*, similarly to the H/C_3N*NS*, distortions can occur in the structures. This deformation in the H/7A-C_3N*NR* is larger rather than that of the H/5Z-C_3N*NR* (see Figs. 9(b,c)). The C-C/C-N bond lengths are elongated to 1.5 Å, and the formed C-H bond lengths are 1.22 and 1.20 Å for the 5Z- and 7A-C_3N*NR*, respectively. In Fig. 9(d,e), we show the optimized geometric structures of H adsorbed on zigzag (6,0)- and armchair (4,4)-C_3N*NT*, respectively, and the diameter and length of (6,0)-C_3N*NT* are 5.147 and 9.062 Å, respectively, and the obtained C-H bond lengths for (6,0)- and (4,4)-C_3N*NT* are 1.104 Å and 1.093 Å respectively. The distortion in the H/(4,4)-C_3N*NT* is larger rather than that of the H/(6,0)-C_3N*NT*.

The electronic band structure of H adsorbed C_3N nanostructures, are shown in Figs. 9(a-e). The band dispersion of the pristine C_3N nanostructures on adsorption of a H adatom at the stable T_C-site is strongly disturbed, due to the covalent-like bonding between the

H adatom and C_3N. The energy bands below and above the E_F are mainly derived from H adatom orbital states and can be described as localized impurity states. In comparison with the pristine C_3NNS, the Dirac-point shape for the H/C_3NNS is greatly changed. The results show that the H/C_3NNS, exhibits a metallic character. The H/5Z- and H/5Z-7A-C_3NNR becomes a ferromagnetic-metal (with 1 μ_B magnetic moment) and a metal, respectively. The spin polarized band structures, and corresponding DOS of the H/(6,0)- and H/(4,4)-C_3NNT, are shown in Figs. 9(d,e). We see that the H/(6,0)-C_3NNT exhibits a dilute-magnetic semiconductor character and induces a magnetic moment of 1 μ_B. The H/(4,4)-C_3NNT is a semiconductor and the H impurity state around E_F can clearly be seen. In comparison with pristine (6,0)- and (4,4)-C_3NNT, the band gap is reduced. To gain more insight into the bond character, the difference charge densities are presented in Figs. 9(a-e). We find a charge accumulation in the region between the H adatom and the neighboring C and N atoms in the region below H, indicating a covalent bond character in the formed H-C bonds. In addition, the difference spin densities are shown for the H/(6,0)-C_3NNT and H/5Z-7A-C_3NNR in the same panel.

VII. EFFECT OF CHARGING AND STRAIN

In this section we present the effect of charging and strain on the properties of the C_3N nanostructures. It is possible to tune the electronic properties by controlling the Fermi energy, E_F, by charging and strain. In Figs. 10(a-e), the variation of the electronic band structure with charging is shown. For q = +0.5 e, the shift in E_F creates holes and in contrast for q = -0.5e, the shift in E_F into the CB gives rise to electrons, resulting in the band gap being dependent on the charging.

With regard to applying strain to the systems, due to the 2D and 1D nature, a greater tolerance to larger strain than the bulk state is possible. Given this characteristic, it is of significant importance to potential applications to investigate the effect of strain in the nanostructures. The tensile and compressive strains are defined as $\varepsilon = (a - a_0)/a_0 \times 100$, where a and a_0 are the strained and non-strained lattice constants of the C_3N nanostructures, respectively. The uniaxial strain is applied along the zigzag direction and the atomic positions are optimized. The electronic band structure under the uniaxial tensile and compressive strains, are shown in Figs. 10(f-j). The range of uniaxial strain is from -8% to $+8\%$. We can see that the band structure is modified with increase or decrease of strain in

C_3N nanostructures, thus it can be seen that the band gap and magnetism is sensitive to structural strain.

VIII. CONCLUSION

Using first-principles calculations, we systematically investigated the structural and electronic properties of the novel 2D nanostructure with a stoichiometry of C_3N which has been recently synthesized. For few-layer C_3N nanosheets (NS) the electronic properties vary with different stacking and layer numbers. Because of the interlayer coupling, the band gap depends on the stacking order between the layers and exhibits monotonically decreasing behavior as the number of layers increases. Furthermore, on application of a uniform electric field, for bilayer $C_3N NS$, the band gap decreases as the electric field changes and a semiconductor-to-metal transition can occur. The effect of nanoribbon width/length and nanotube length/diameter on the electronic structure were also investigated where it was found that the electronic structure can be modified depending on these dimensions, length and diameter. We also considered the adsorption of H atoms on the C_3N nanostructures and found it can lead to considerable changes in the electronic structure if the related adsorption energy is significant. Under these conditions, either the band gap can be reduced or diminished and the system becomes metallic or semiconducting and magnetism may also be induced. Our results show that the band gap and magnetic moment, with applied charging, electric field and strain, exhibit considerable changes. Thus, it is possible to tune the electronic and magnetic properties of C_3N nanostructures. Importantly, the existence of a tunable band gap and magnetism in C_3N nanostructures is highly desirable for its use in nanoscale device applications.

IX. ACKNOWLEDGMENTS

In addition, we acknowledge OpenMX team for OpenMX code.

X. KEYWORDS

C_3N nanostructures, Nanosheet, Nanotube, Nanoribbon, Electronic properties, first-principles

XI. TOC

Ab initio calculations for the recently synthesised two-dimensional carbon nitride material, C_3N, in various nanostructures, including nanoribbons, nanotubes, nanosheets and multilayers, show that the electronic and magnetic properties can be very diverse, and that by application of strain, electric field, charging, and H atom adsorption these properties can be changed to induce a metallic, half-metallic, semiconducting and magnetic behaviour. Thus, this new family of C_3N nanostrucures may hold great potential in applications such as sensors, electronics and optoelectronic technologies.

* catherine.stampfl@sydney.edu.au

[1] F. K. Kessler, Y. Zheng, D. Schwarz, C. Merschjann, W. Schnick, Wang, M. J. Bojdys, *Nat. Rev. Mater.* **2017**, *2*, 17030.

[2] J. Zhang, Y. Chen, X. Wang, *Energy Environ. Sci.* **2015**, *8*, 3092-3108.

[3] Q. Zhou, M. Wu, M. Zhang, G. Xu, B. Yao, Ch. Li, G. Shi, *Materials Today Energy* **2017**, *6*, 181-188.

[4] S. U. Lee, R. V. Belosludov, H. Mizuseki, Y. Kawazoe, *Small* **2008**, *5*,1769-1775.

[5] J. Li, W. Cui, Y. Sun, Y. Chu, W. Cen, F. Dong, *J. Mater. Chem. A* **2017**, *5*, 9358-9364.

[6] Y. Zheng, J. Liu, J. Liang, M. Jaroniec, Sh. Zh. Qiao, *Energy Environ. Sci.* **2012**, *5*, 6717-6731.

[7] J. Mahmood, E. K. Lee, M. Jung, D. Shin, I.-Y. Jeon, S.-M. Jung, H.-J. Choi, J.-M. Seo, S.-Y. Bae, S.-D. Sohn, N. Park, J. H. Oh, H.-J. Shin, J.-B. Baek, *Nat. Commun.* **2015**, *6*, 6486.

[8] B. Mortazavi, O. Rahaman, T. Rabczuk, L. F. C. Pereira *Carbon* **2016**, *106*, 1-8.

[9] G. Zhu, K. L, Q. Sun, Y. Kawazoe, P. Jena, *Comput. Mater. Sci.* **2014**, *81*, 275-279.

[10] X. Li, Sh. Zhang, Q. Wang, *Phys. Chem. Chem. Phys.* **2013**, *15*, 7142-7146.

[11] E. Kroke, M. Schwarz, E. Horath-Bordon, P. Kroll, B. Noll, A. D. Norman, *New J. Chem.* **2002**, *26*, 508-512.

[12] A. J. Mannix, B. Kiraly, M. C. Hersam, N. P. Guisinger, *Nature Reviews Chemistry* **2017**, *1*, 0014.

[13] A. Du, S. Sanvito, S. C. Smith, *Phys. Rev. Lett.* **2012**, *108*, 197207.

[14] J. S. Lee, X. Wang, H. Luo, S. Dai, *Adv. Mater.* **2010**, *22*, 1004-1007.

[15] Q. Guo, Q. Yang, Ch. Yi, L. Zhu, Y. Xie, *Carbon* **2005**, *43*, 1386-1391.

[16] J. Li, Ch. Cao, J. Hao, H. Qiu, Y. Xu, H. Zhu, *Diamond and Related Mater.* **2006**, *15*, 1593 - 1600.

[17] H. Qiu, Zh. Wang, X. Sheng, *Phys. Lett. A.* **2013**, *377*, 347-350.

[18] A. Wang, X. Zhang, M. Zhao, *Nanoscale* **2014**, *6*, 11157-11162.

[19] J. Wirth, R. Neumann, M. Antonietti, P. Saalfrank, *Phys. Chem. Chem. Phys.* **2014**, *16*, 15917-15926.

[20] X. Zhang, M. Zhao, A. Wang, X. Wang, A. Du, *J. Mater. Chem. C* **2013**, *1*, 6265-6270.

[21] X. Wang, K. Maeda, A. Thomas, K. Takanabe, G. Xin, J. M. Carlsson, K. Domen M. Antonietti, *Nat. Mater.* **2008**, *8*, 76.

[22] I. Choudhuri, G. Bhattacharyya, S. Kumar, B. Pathak, *J. Mater. Chem. C* **2016**, *4*, 11530-11539.

[23] A. Thomas, A. Fischer, F. Goettmann, M. Antonietti, J.-O. Mller, R. Schlgl, J. M. Carlsson, *J. Mater. Chem.* **2008**, *18*, 4893-4908.

[24] G. Algara-Siller, N. Severin, S. Y. Chong,T. Bjrkman, R. G. Palgrave, A. Laybourn, M. Antonietti, Y. Z. Khimyak, A. K. Krasheninnikov, J. P. Rabe, U. Kaiser, A. I. Cooper, A. Thomas, M. I. Bojdys, *Angewandte Chemie* **2014**, *126*, 7580-7585.

[25] D. Mpoutas, L. Tsetseris, *Phys. Chem. Chem. Phys.* **2017**, *19*, 26743-26748.

[26] L. Tsetseris, *Phys. Chem. Chem. Phys.* **2016**, *18*, 26088-26093.

[27] L. Li, X. Kong, O. Leenaerts, X. Chen, B. Sanyal, F. M. Peeters, *Carbon* **2017**, *118*, 285-290.

[28] Ch. Pu, D. Zhou, Y. Li, H. Liu, Zh. Chen, Y. Wang, Y. Ma, *Phys. Chem. C* **2017**, *121*, 2669-2674.

[29] H. Chen, Sh. Zhang, W. Jiang, Ch. Zhang, H. Guo, Zh. Liu, Zh. Wang, F. Liu, X. Niu, *J. Mater. Chem. A* **2018**, *6*, 11252-11259.

[30] H. Li, H. Hu, Ch. Bao, J. Hua, H. Zhou, X. Liu, X. Liu, M. Zhao, *Phys. Chem. Chem. Phys.* **2015**, *17*, 6028-6035.

[31] X. Zhang, A, Wang, M. Zhao, *Carbon* **2015**, *84*, 1-8.

[32] L. Huang, Z. Liu, W. Chen, D. Cao, A. Zheng, *J. Mater. Chem. A* **2018**, *6*, 7168-7174.

[33] W. H. Brito, J. da Silva-Ara, H. Chacham, *J. Phys. Chem. C* **2015**, *119*, 19743-19751.

[34] L. Z. Liu, X. L. Wu, X. X. Liu, P. K. Chu, *Phys. Lett.* **2015**, *106*, 132406.

[35] H. Sahin, *Phys. Rev. B* **2015**, *92*, 085421.

[36] C. N. M. Ouma, K. O. Obodo, M. Braun, G. O. Amolo, *J. Mater. Chem. C* **2018**, *6*, 4015-4022.

[37] J. Mahmood, E. K. Lee, M. Jung, D. Shin, H.-J. Choi, J.-M. Seo, S.-M. Jung, D. Kim, F. Li, M. S. Lah, N. Park, H.-J. Shin, J. H. Oh, J.-B. Baek, *PNAS* **2016**, *113*, 7414.

[38] Q. Hu, Q. Wu, H. Wang, J. He, G. Zhang, *physica status solidi (b)* **2011**, *294*, 784-788.

[39] S. Mizuno, M. Fujita, K. Nakao, *Synthetic Metals* **1995**, *71*, 1869 - 1870.

[40] M. Yagmurcukardes, S. Horzum, E. Torun, F.M. Peeters, R. T. Senger, *Phys. Chem. Chem. Phys.* **2016**, *18*, 3144-3150.

[41] Y. Z. Abdullahi, T. L. Yoon, Th. L. Lim, *Mater. Res. Exp.* **2019**, *6*, 025601.

[42] B. Mortazavi, *Carbon* **2017**, *118*, 25-34.

[43] M.-Y. Chang, Ch.-S. Wu, Y.-F. Chen, B.-Z. Hsieh, W.-Y. Huang, K.-Sh. Ho, T.-H. Hsieh, Y.-K. Han, *Organic Electronic* **2008**, *9*, 1136 - 1139.

[44] M. M. Alam, J. Wang, Y. Guo, S. P. Lee, H.-R. Tseng, *J. Phys. Chem. B* **2005**, *109*, 12777-12784.

[45] J. Xu, J. Mahmood, Y. Dou, Sh. Dou, F. Li, L. Dai, J. B. Baek, *Adv. Mater.* **2017**, *29*, 1702007.

[46] A. Bafekry, S. Farjami Shayesteh, F. M. Peeters, *Phys. Chem. C* **2019**, *123*, 12485.

[47] M. B. Tagani, S. I. Vishkayi, *Appl. Phys.* **2018**, *124*, 084304.

[48] A. Bafekry and M. Ghergherehchi and S. Farjami Shayesteh and F.M. Peeters, *Chemical Physics* **2019**, *526*, 110442.

[49] M. B. Tagani, *Comput. Mater. Sci.* **2018**, *153*, 126-133.

[50] A. Bafekry, C. Stampfl, S. Farjami Shayesteh, and F. M. Peeters, *Adv. Elec. Mater.* **2019**, , 1900459.

[51] Zh. Wu, H. Zhang, J. Lin, J. Zhao, X. Cheng, *Chemical Physics* **2020**, *528*, 110471.

[52] A. Bafekry, S. Farjami Shayesteh, and F. M. Peeters, *Phys. Chem. Chem. Phys.* **2019**, *21*, 21070.

[53] Z. Golsanamlou, M. B. Tagani, H. R. Soleimani, *Phys. Chem. Chem. Phys.* **2015**, *17*, 13466-13471.

[54] A. K. Geim, K. S. Novoselov, *Nat. Mater.* **2007**, *6*, 183-191.

[55] H. Guo, N. Lu, J. Dai, X. Wu, X. C. Zeng, *J. Phys. Chem. C* **2014**, *118*, 14051-14059.

[56] P. F. Yuan, Z. Q. Fan, Z. H. Zhang,

[57] B. Akgenc, *Computational Materials Science* **2020**, *171*, 109231.

[58] A. Bafekry, M. Ghergherehchi, and S. Farjami Shayesteh, *Phys. Chem. Chem. Phys.* **2019**, *21*, 10552.

[59] M. Yagmurcukardes, F. M. Peeters, R. T. Senger, H. Sahin, *Applied Physics Reviews* **2016**, *3*, 041302.

[60] Y. Xie, Ch. Gong, J. Zhou, X. Yan, Y. Chen, Design triple points, nexus points, and related topological phases by stacking monolayers, *Appl. Phys. Lett.* **2019**, *115*, 073105

[61] A. Bafekry, M. Ghergherehchi, S. Farjami Shayesteh, F. M. Peeters, *Appl. Phys.* **2019**, *126*, 144304.

[62] B. Akgenc, *J. Mater. Sci.* **2019**, *54*, 95439552

[63] D Kiymaz, M Yagmurcukardes, A Tomak, H Sahin, R T Senger, F M Peeters, H M Zareie, and C Zafer Controlled growth mechanism of poly (3-hexylthiophene) nanowires. *Nanotechnology* **2016**, *27*, 455604.

[64] A. Bafekry, B. Mortazavi, and S. Farjami Shayesteh *Journal of Magnetism and Magnetic Materials* **2019**, *491*, 165565.

[65] B. Akgenc, *Solid State Communications* **2019**, *303-304*, 113739.

[66] A. Bafekry, Catherine Stampfl, Mitra Ghergherehchi, S. Farjami Shayesteh *CARBON* **2019**, .

[67] M. Yagmurcukardes, *Phys. Rev. B* **2019**, *100*, 024108.

[68] A. Bafekry, B. Akgenc, S. Farjami Shayesteh, B. Mortazavi, *Appl. Surf. Sci.* **2019**, .

[69] J. P. Perdew, K. Burke, M. Ernzerhof, *Phys. Rev. Lett.* **1996**, *77*, 3865-3868.

[70] N. Troullier, J. L. Martins, *Phys. Rev. B* **1991**, *43*, 1993-2006.

[71] T. Ozaki, *Phys. Rev. B* **2003**, *67*, 155108.

[72] T. Ozaki, T. and Kino, H. *Phys. Rev. B* **2004**, *69*, 195113.

[73] H. J. Monkhorst, J. D. Pack, *Phys. Rev. B* **1976**, *13*, 5188-5192.

[74] J. Tersoff, D. R. Hamann, *Phys. Rev. Lett.* **1983**, *50*, 1998-2001.

[75] I. Horcas, R. Fernndez, J. M. Gmez-Rodrguez, J. Colchero,J. Gmez-Herrero, A. M. Baro, *Review of Scientific Instruments* **2007**, *78*, 013705.

[76] Paolo Giannozzi, Stefano Baroni, Nicola Bonini, Matteo Calandra, Roberto Car, Carlo Cavazzoni, Davide Ceresoli, Guido L Chiarotti, Matteo Cococcioni, Ismaila Dabo, An- drea Dal Corso, Stefano de Gironcoli, Stefano FabrisGuido Fratesi, Ralph Gebauer, Uwe Gerstmann, Chris- tos Gougoussis, Anton Kokalj, Michele Lazzeri, Layla Martin-Samos, Nicola

Marzari, Francesco Mauri, Riccardo Mazzarello, Stefano Paolini, Alfredo Pasquarello, Lorenzo Paulatto, Carlo Sbraccia, Sandro Scandolo, Gabriele Sclauzero, Ari P Seitsonen, Alexander Smogunov, Paolo Umari, and Renata M Wentzcovitch. *J. Physics: Condensed Matter* **2009**, *21*, 395502.

[77] H. J. Xiang, B. Huang, Z. Y. Li, S.-H. Wei, J. L. Yang, X. G. Gong, *Phys. Rev. X* **2012**, *2*, 011003.

[78] W. Li, X. Dai, J. Morrone, G. Zhang, R. Zhou, *Nanoscale* **2017**, *9*, 12025-12031.

[79] L.-B. Shi, Y.-Y. Zhang, X.-M. Xiu, H.-K. Dong, *Carbon* **2018**, *134*, 103-111.

[80] S. Azevedo, M. Machado, J. R. Kaschny, *Appl. Phys. A* **2011**, *104*, 55-60.

[81] Z. Huang, F. Li, B. Chen and G. Yuan, *RSC Advances*, **2015**, *5*, 102700-102706.

[82] X. Wang, C. Zhou, R. Shi, Q. Liu, G. I. N. Waterhouse, L. Wu, C.-H. Tung and T. Zhang, *Nano Research*, **2019**, *12*, 2385-2389.

[83] R. Czerw, M. Terrones, J.-C. Charlier, X. Blase, B. Foley, R. Kamalakaran, N. Grobert, H. Terrones, D. Tekleab, P. Ajayan, *Nano Lett.* **2001**, *1*, 457-460.

[84] J. Hales, A.S. Barnard, *J. Phys. Cond. Mat.* **2009**, *21*, 144203-144207.

[85] E. Kim, C. Chen, T. Kahler, M. Elstner, T. Frauenheim, *Phys. Rev. B* **2001**, *64*, 094107.

[86] A. Sandre, C.J. Pickard, C. Colliex, *Chem. Phys. Lett.* **2000**, *325*, 53-60.

[87] S. Azevedo, R. De Paiva, Structural stability and electronic properties of carbon- boron nitride compounds, *Europhys. Lett.* **2006**, *75*, 126.

[88] S. Jalili, F. Molani, M. Akhavan, J. Schofield, *Phys. E* **2014**, *56*, 48-54.

[89] Z. Bagheri, *Phys. E* **2016**, *76*, 151-157.

[90] M. Pashangpour, A. A. Peyghan, *J. Mol. Model.* **2015**, *21*, 116.

[91] z. Rostami, a. Bodaghi, *J. Mol. Liq.* **2016**, *220*, 687-692.

[92] F. Molani, S. Jalili, J. Schofield, Hydrogen *Energy* **2016**, *41*, 7431-7437.

[93] M. Eslami, M. Moradi, R. Moradi, *Vacuum* **2016**, *133*, 7-12.

10.1002/cphc.201900852

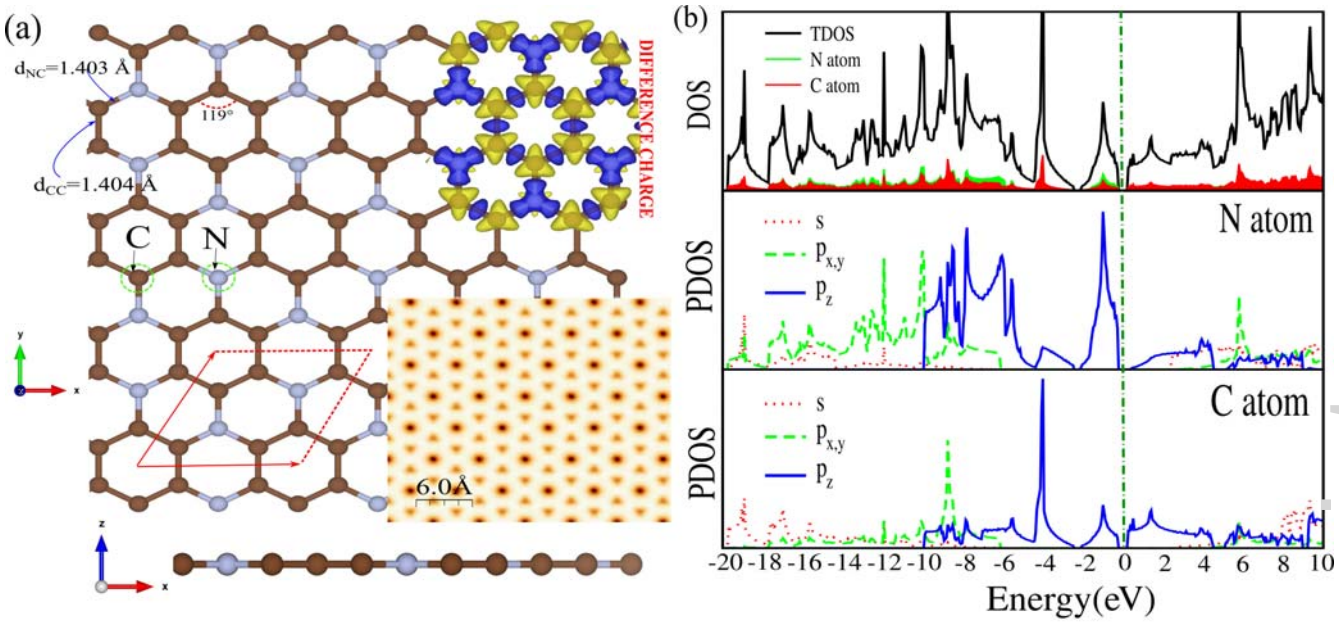

Figure 1. (a) The optimized atomic structure of C_3N, indicated by a red parallelogram. Difference charge density and simulated STM images are shown in the same panel. The blue and yellow regions represent charge accumulation and depletion, respectively. The blue (brown) balls indicate N (C) atoms. (b) DOS and PDOS of C and N atoms. The zero of energy is set to the Fermi energy (E_F).

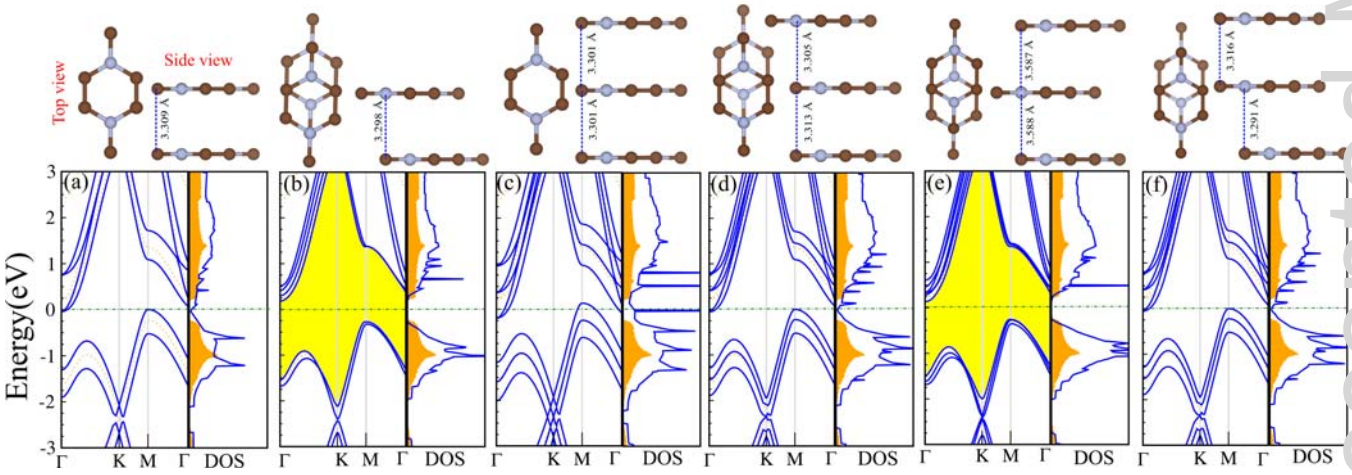

Figure 2. The optimized atomic structures, band structure, DOS and PDOS of few layer C_3N nanosheet with different stackings. The zero of energy is set to the Fermi level energy.

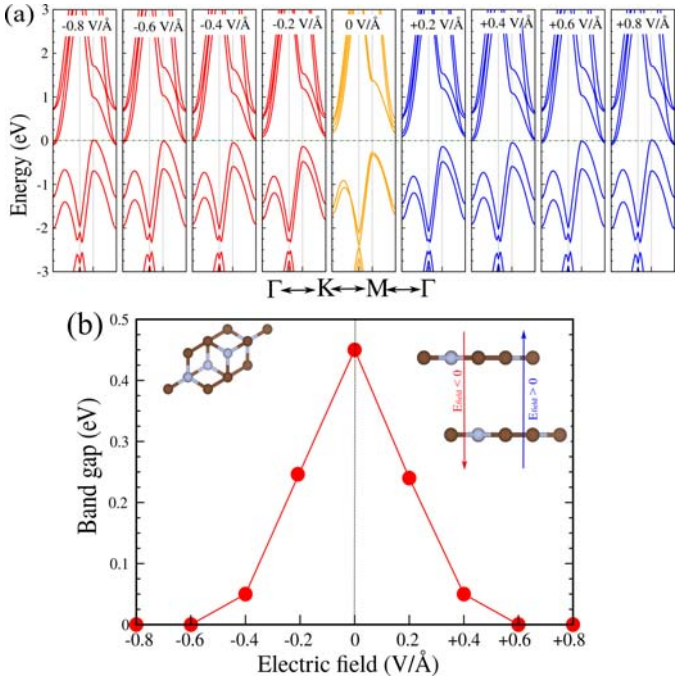

Figure 3. (a) Electronic structure of bilayer C_3NNS as a function of the applied electric field, whose strength varies from -0.8 to +0.8 V/Å. The perpendicular electric field, namely $\mathbf{F} > 0$ and < 0 which denotes parallel and antiparallel to the z-axis, respectively. (b) Band gap of bilayer C_3NNS with respect to the electric field. The zero of energy is set at the E_F.

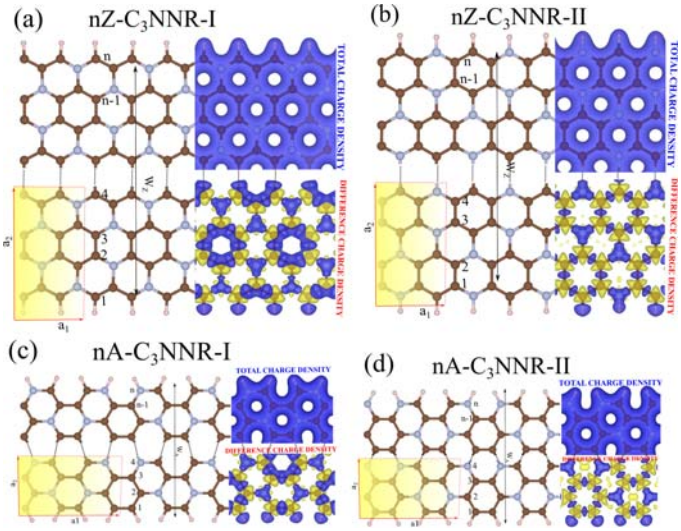

Figure 4. Atomic structures of H-passivated (a,b) zigzag and (c,d) armchair C_3N nanoribbons with two types of atomic arrangements (I and II). The C, N and H atoms are represented by brown, gray and white spheres, respectively. The C_3NNR are periodic along the y-direction. The unit cell of the C_3NNR is indicated by dashed rectangular boxes. The total and difference charge density are also shown in the same panel.

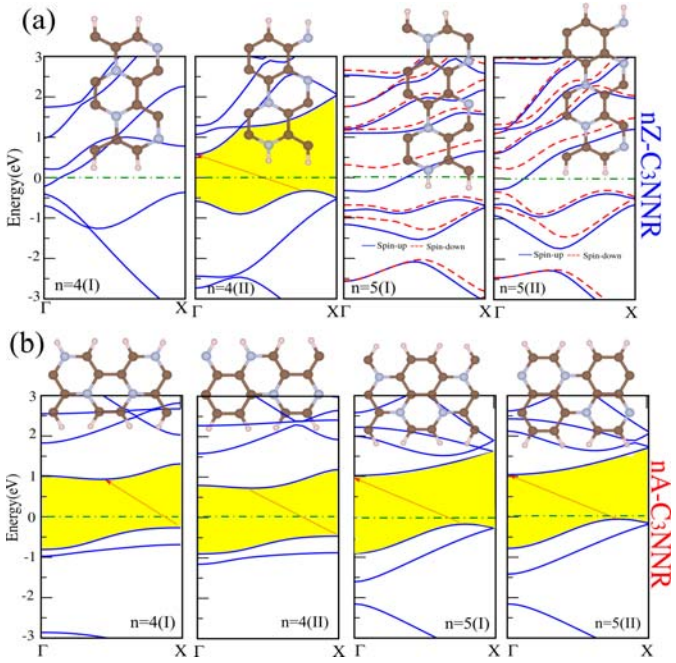

Figure 5. Optimized atomic and electronic structure of H-passivated (a) nZigzag- and, (b) nArmchair-C_3N nanoribbons with n= 4 and 5 in the I and II configurations. The top view of the optimized structures are shown in the insets. The C, N and H atoms are represented by brown, gray and white spheres, respectively. The zero of energy is set at the E_F.

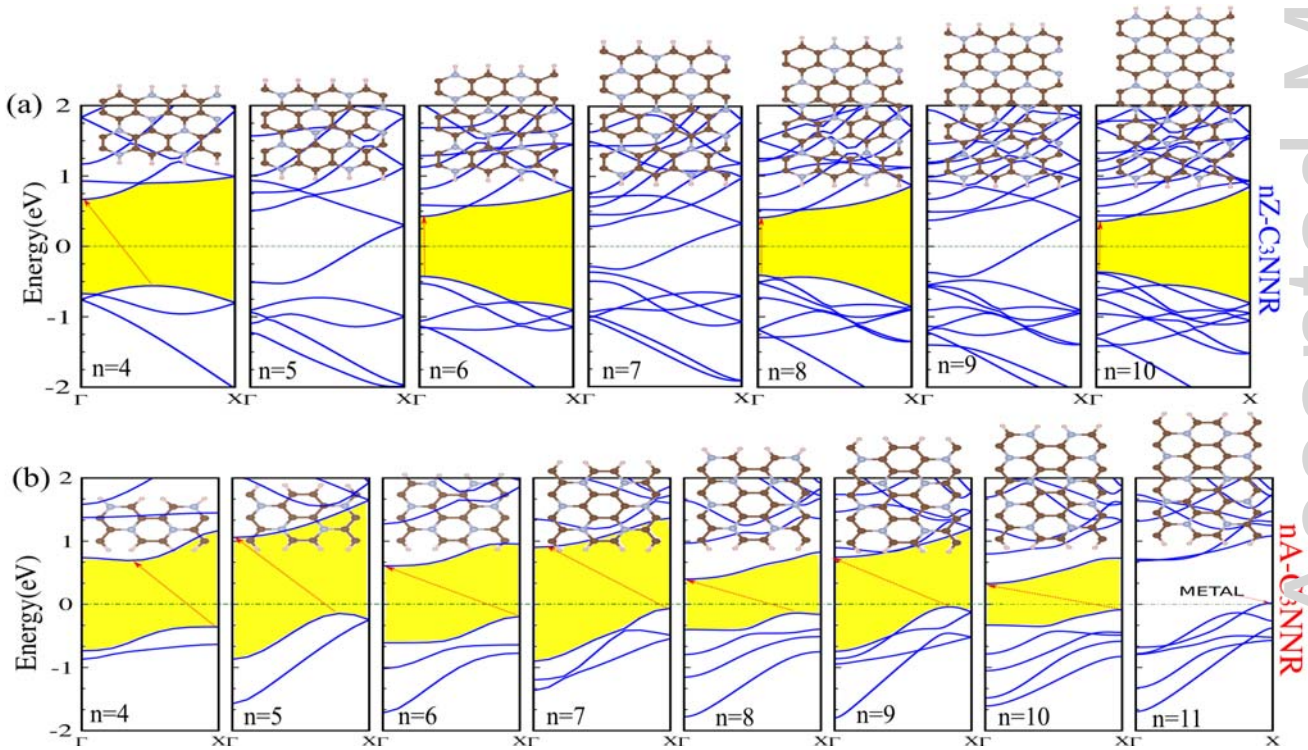

Figure 6. Electronic structure of H-passivated (a) nZigzag- and (b) nArmchair-C_3N nanoribbons with n=1-14 in the I configuration. The top view of the optimized atomic structures are shown in the insets. The C, N and H atoms are represented by brown, gray and white spheres, respectively. The zero of energy is set at the E_F.

10.1002/cphc.201900852

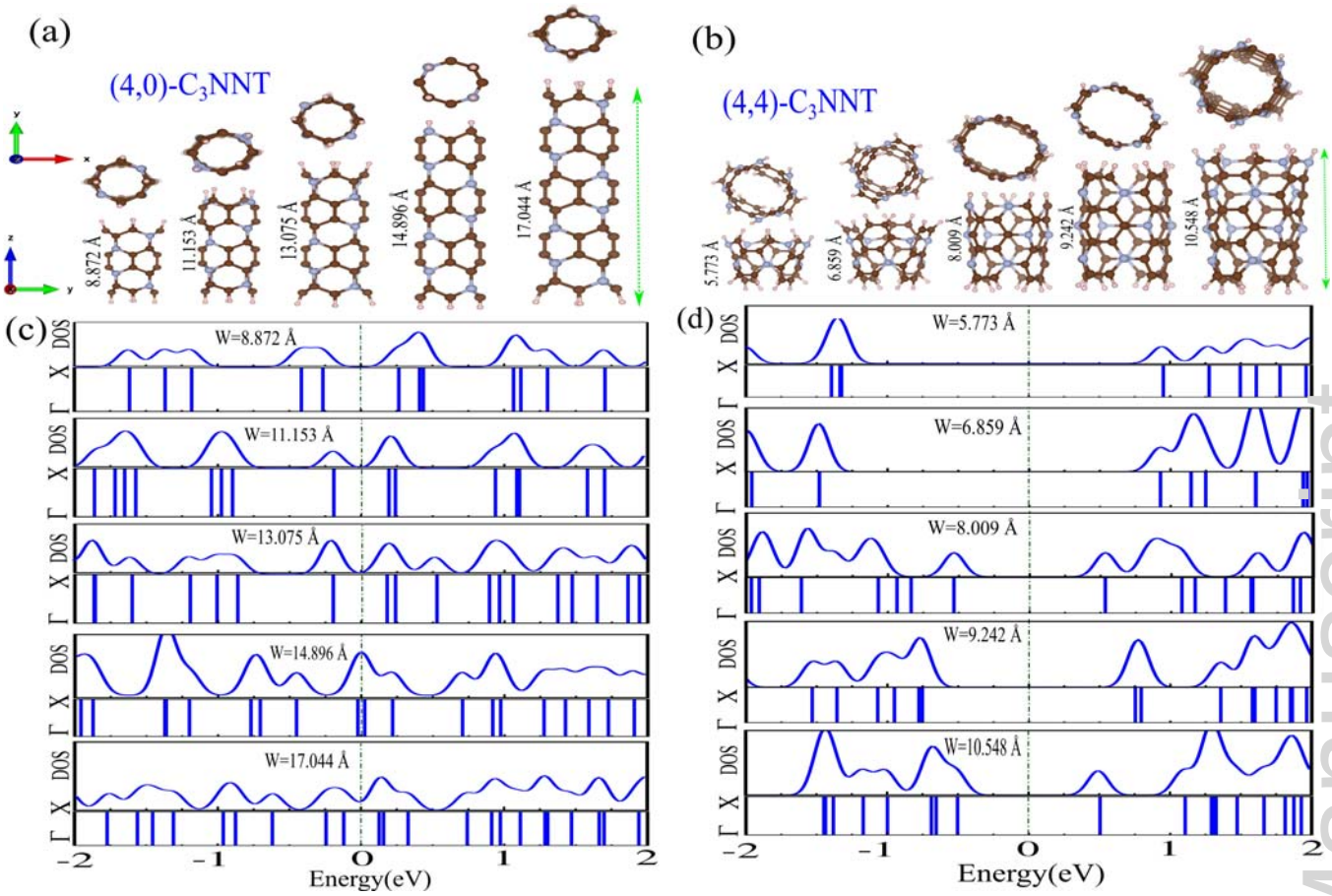

Figure 7. Optimized atomic and electronic structures of (a,b) (4,0)-C_3N and (c,d) (4,4)-C_3N nanotubes passivated with H atoms as a function of the nanotube length. The zero of energy is set at the E_F.

10.1002/cphc.201900852

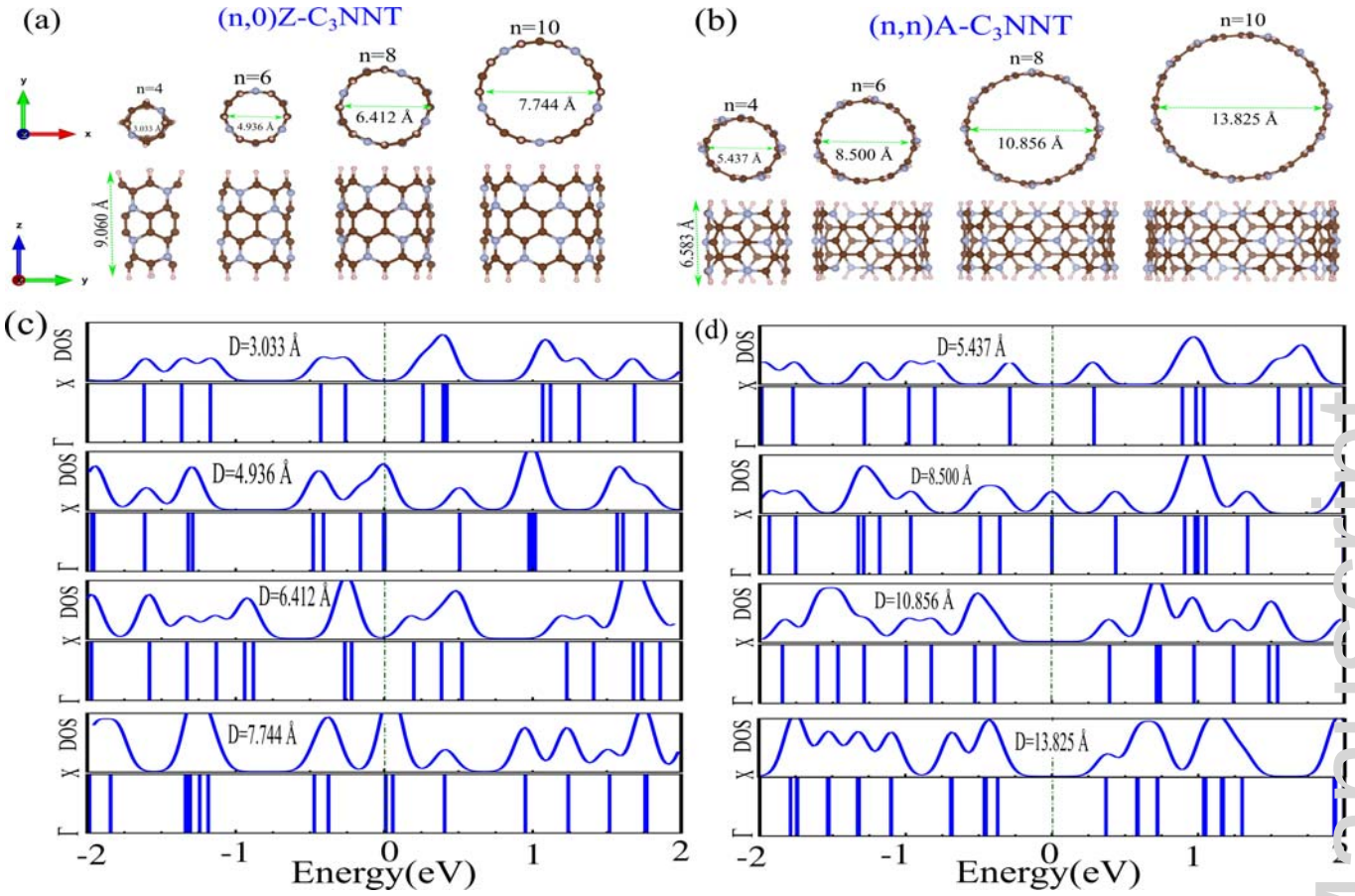

Figure 8. The optimized atomic and electronic structures of (a,b) (4,0)-C_3N and (c,d) (4,4)-C_3N nanotubes passivated with H atoms as a function of the nanotube diameter. The zero of energy is set at the E_F.

10.1002/cphc.201900852

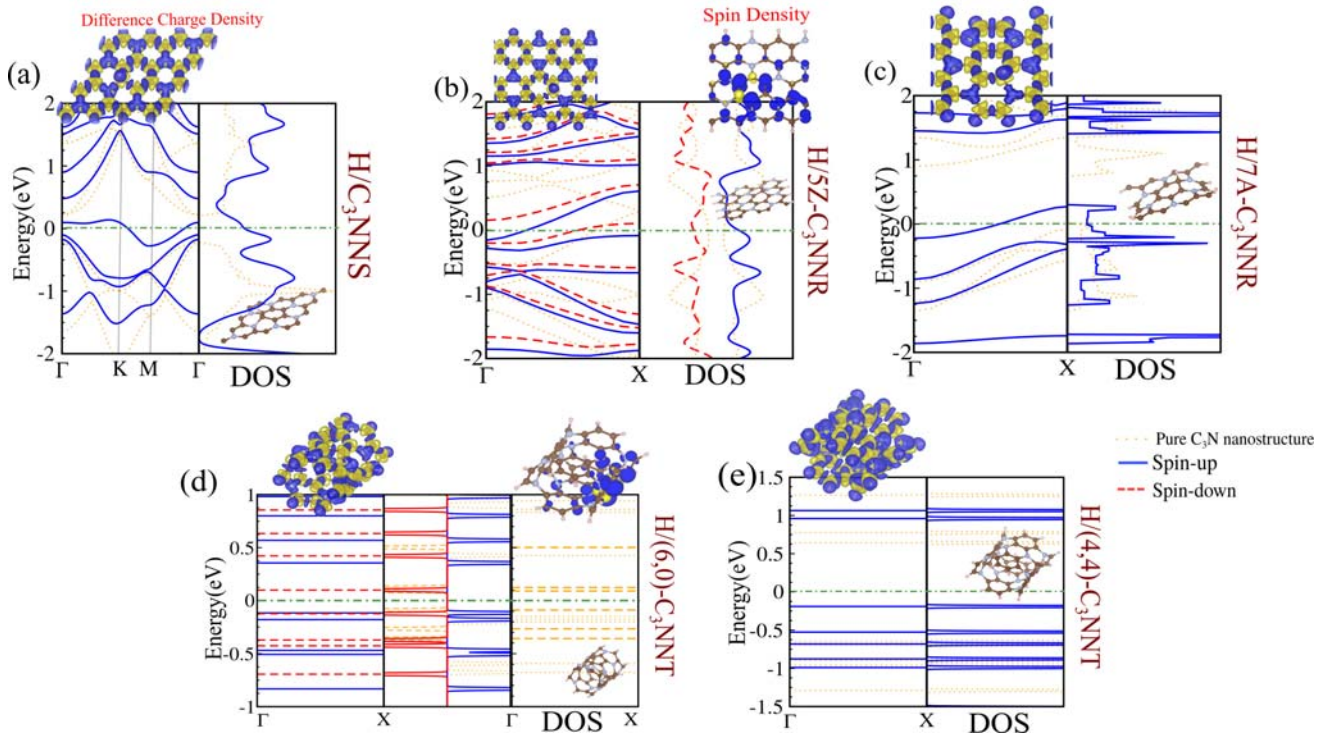

Figure 9. (a-e) The band structure and DOS for the adsorption of a H atom on (a) the C_3NNS, (b) 5Z-C_3NNS, (c) 7A-C_3NNR, (d) (6,0)-C_3NNT and (e) (4,4)-C_3NNT. The total charge densities are shown in same panel. The difference spin density is indicated in the same panel. The positive and negative regions of difference density are represented by blue and yellow, respectively. The zero of energy is set at the E_F.

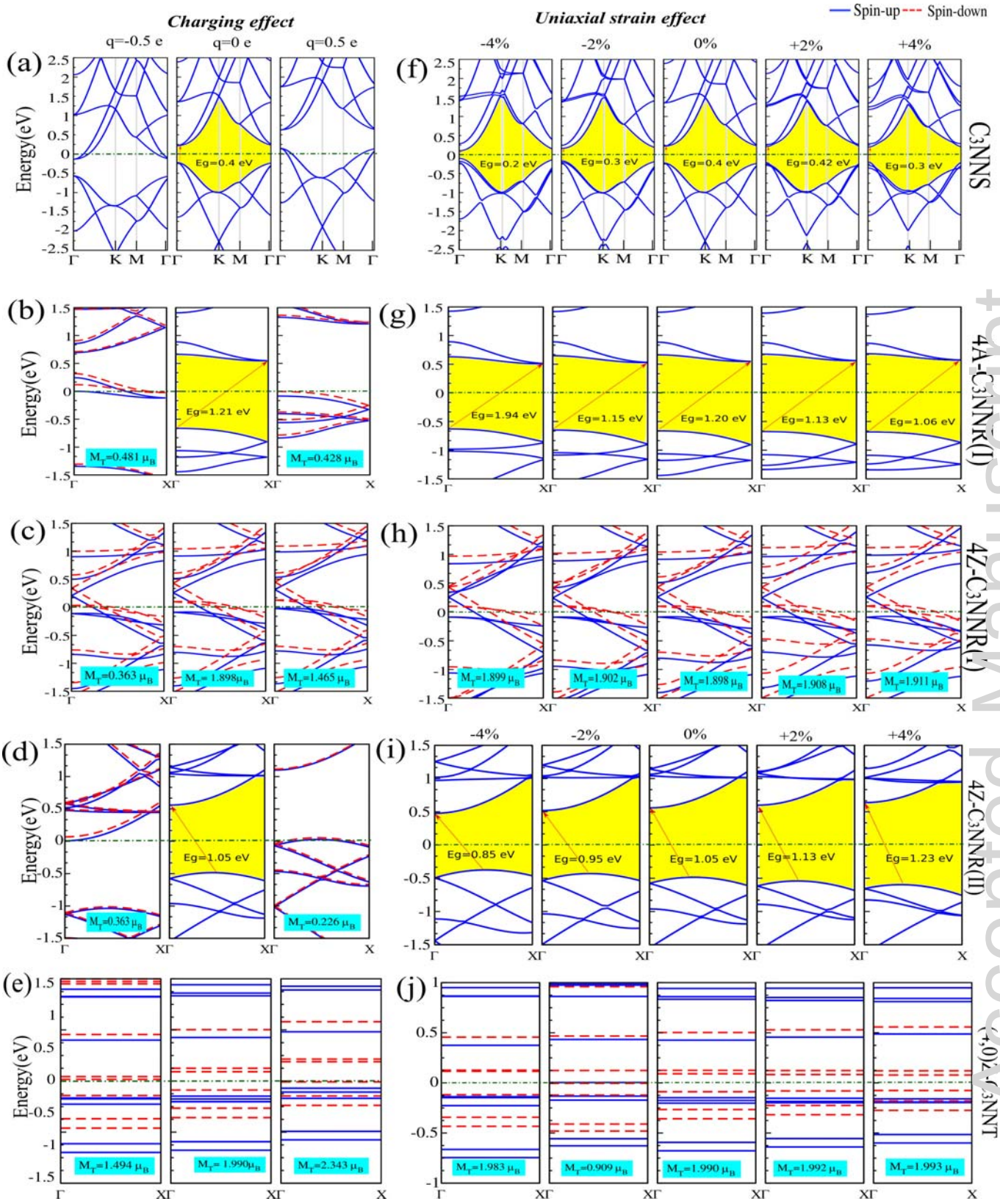

Figure 10. Electronic structure of the C_3N (a) nanosheet, (b-d) nanoribbon and (e) nanotube as a function of charging. Electronic structure of the C_3N (f) nanosheet, (g-i) nanoribbon and (j) nanotube as a function of the strain. q= +0.5 e and q= -0.5 e, corresponds to the charging where one electron is removed from, and added to, the C_3N nanostructures, respectively. The zero of energy is set at E_F.